Triple ion beam irradiation of glass-ceramic materials for nuclear fusion technology

Triple ion beam irradiation of glass-ceramic materials for nuclear fusion technology

Daniele Torsello[a,b], Valentina Casalegno[a], Giorgio Divitini[c,d], Gianluca Ghigo[a,b], Roberto Gerbaldo[a,b], Michela Fracasso[a,b], Fabiana D'Isanto[a], May Ching Lai[c], Laurent Roux[e], Gaelle Gutierrez[e], Caterina Ducati[c], Celine Cabet[e], Monica Ferraris[a], Laura Gozzelino[a,b]

[a]*Department of Applied Science and Technology, Politecnico di Torino, I-10129 Torino, Italy*
[b]*Istituto Nazionale di Fisica Nucleare, Sezione di Torino, I-10125 Torino, Italy*
[c]*Department of Materials Science & Metallurgy, University of Cambridge, CB30FS, Cambridge, UK*
[d]*Istituto Italiano di Tecnologia, 16163 Genova, Italy*
[e]*Université Paris-Saclay, CEA, Service de Recherches de Métallurgie Physique, 91191, Gif-sur-Yvette, France*

Abstract

The analysis of the radiation damage associated with energetic neutrons is a key factor for the application of glass-ceramics as joining materials in nuclear fusion plants. Triple ion beam irradiation is, currently, the only way to emulate the displacement damage and the effects of transmutation products induced by high energy neutrons at elevated doses by producing a high level of displacements per atom (dpa) and implanting high concentrations of low solubility gases on the glass-ceramic microstructure. In this paper, we investigate calcia-alumina glass-ceramics in which the damage expected in the working conditions of a nuclear fusion plant were reproduced by simultaneous irradiation with Si, He and H ions at different temperatures. TEM analysis of irradiated calcia-alumina samples shows a complete amorphization of the irradiated portion and the formation of He bubbles/cavities. The irradiation temperature plays a prominent role in determining the induced damage in terms of recrystallization, phase mixing and bubble density and aggregation.

Keywords: triple ion beam irradiation, glass-ceramics, nuclear fusion technology, neutron damage, temperature effect

1. Introduction

Materials operating within a fusion reactor will be exposed to severe conditions, including high temperature and long-term irradiation by high-energy (up to 14 MeV) neutrons [1]. For this reason, it is necessary to develop new materials with excellent performances in extreme radiation environments [2, 3].

Ceramic-matrix composites (CMCs) are considered a key component to guarantee the performance and safety of nuclear fusion (and also fission) reactors. The use of composite materials as cladding or structural materials in the nuclear plants is based on strict requirements. In the case of fusion reactors, CMCs are candidate materials for plasma-facing components, both as complete structures and components thereof [4], which will be exposed to both a high heat flux and a high energy neutron flux. This proposal is based on a series of promising reports on the irradiation performances of SiC based CMCs that highlighted their low activation, high temperature endurance capability, relatively low neutron activation, excellent chemical stability and radiation resistance [5]. However, as performance data collects, the limitations of the current generation of nuclear-grade SiC based materials are becoming more evident; this particularly applies for SiC composites [6]. A number of options for improving the performance of the next generation of SiC composites were reported in [7], starting from the results on neutron irradiation resistance. Still, several technical challenges must be addressed for the realization of SiC-based materials for use in fusion energy systems, and the development of joining technology is one of the most critical [8, 9]. In fact, SiC based materials, as well CMCs in general, do not melt and they cannot be welded by ordinary methods; furthermore, the mechanical joints produced using ceramic connection (mechanical fasteners, screws, bolts, etc.) are not always tight. Preferably, CMCs should be joined by localized heating of the joining area and no pressure should be applied to obtain the joint, thus increasing the possibility of connecting complex and non-flat components. Glasses and glass-ceramics can fulfil most of the requirements to join CMCs to themselves and to other materials [10].

In this framework, in the last decade we focused on low-activation glass-ceramics based on calcia-alumina (CaO-Al_2O_3, CA), silica-alumina-yttria (SiO_2-Al_2O_3-Y_2O_3, SAY) and silica-alumina-magnesia (SiO_2-Al_2O_3-MgO, SAMg), that show potential as SiC/SiC indirect joining materials [11, 12]. These glass-ceramics have been used to join SiC based materials (both monolithic SiC and SiC based composites) through the so-called "glass-ceramic method", that yields "self-healing" joints that can heal cracks via heating above their softening temperature. First radiation hardness tests under fission neutron and ion irradiations gave promising results [13, 14, 15, 16], but the knowledge of the effects of radiation damage associated with energetic neutrons is still lacking, especially in the extreme conditions expected in fusion reactors.

The reference neutron energy for nuclear fusion plants is 14 MeV (resulting from the reaction between deuterium and tritium), and high doses are expected due to the intense flux and

long exposition times. These extreme conditions represent an issue in the possibility to investigate the response of materials to the working environment since no experimental facility allows obtaining a high intensity flux of such energetic neutrons. Therefore, the radiation hardness can be investigated either employing high doses of lower energy neutrons, or by a combination of ion irradiations that emulate the expected damage produced by 14 MeV neutrons. The problem with the former approach is that the yield of transmutation elements (mainly He and H for our material) is much smaller at low neutron energies and therefore such experiments neglect one important source of properties modification. With the latter approach it is possible to emulate the expected ratio between displacement damage (dpa) and transmutation elements yield by employing a simultaneous irradiation with heavy ions. These irradiations provide the necessary dpa, and light ions, that can be implanted in the expected amount and that could result in the formation of bubbles [17, 18].

Such experiments need to be carefully guided by Monte Carlo simulations to: (i) calculate the expected damage from high energy neutron exposure, and (ii) decide the best combination of ion irradiation conditions to reproduce the calculated damage.

In this paper, we study by transmission electron microscopy (TEM) analysis the effects of triple ion beam irradiation on calcia-alumina. The irradiation conditions were chosen to emulate the expected neutron damage after 0.75 years of exposition to 14 MeV neutrons delivering a power density of 3 MW/m^2 as expected in the working conditions of the first wall of DEMO [19]. To the best of our knowledge, this is the first report of high temperature multi-beam irradiation experiments on glass-ceramics.

2. Monte Carlo simulations

Monte Carlo simulations with pre-compiled codes are an extremely useful tool to investigate radiation damage and guide experimental investigations. In this paper, we employed the PHITS code [20] to compute the expected damage in CA exposed to 14 MeV neutrons in terms of dpa, He and H yield and their ratios. The SRIM code [21] (unable to simulate neutron-matter interaction but the most commonly used code for ion-matter interaction) was then employed to decide the combination of the three ion beams that would best reproduce the ratios calculated with PHITS.

The details of the target material were the same in both codes: the density was 3.04 g/cm^3 (experimentally determined) and the atomic percentage composition 20.9% Ca, 23.2% Al and 55.8% O. A threshold displacement energy of 25 eV was assumed for all the elements.

2.1. Neutron damage - PHITS

The PHITS code (version 3.02) was employed with the event-generator mode to compute the damage produced by 14 MeV neutrons on CA in terms of dpa and H and He transmutation products. All results are normalized on the number of impinging neutrons, so that they can be rescaled to achieve the expected values for a specific dose (operation time). What is most relevant for the experiments is then the ratio between dpa and transmutation products. The obtained results are summarized in Table 1.

Quantity	Value
dpa/n	$2.19\times10^{-23} \pm 0.04\times10^{-23}$
He/(cm^3 n)	$1.30\times10^{-4} \pm 0.07\times10^{-4}$
H/(cm^3 n)	$7.6\times10^{-6} \pm 1.8\times10^{-6}$

Table 1: Neutron damage parameters for 14 MeV neutrons on CA obtained by PHITS simulations.

2.2. Ion irradiation - SRIM

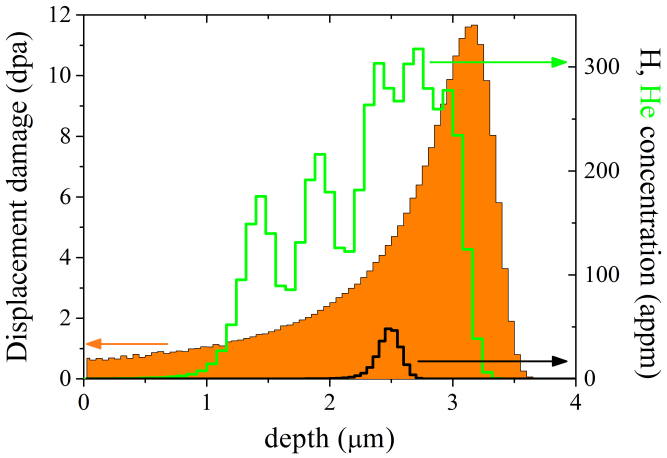

Figure 1: Displacement damage calculated in CA for 8 MeV Si irradiation (orange histogram) and He- and H-ion distributions calculated for 2 MeV He-ions (green line) without (not shown, positioned at 5.5 μm) and with 5 different energy degraders and 0.33 MeV H-ions (black line), respectively.

Starting from the data reported in Table I and from the predicted flux of 14 MeV neutron in correspondence to the first wall [19], we tried reproducing in a slice of the sample a similar displacement and transmutation damage by a suitable choice of ions, energy and fluence. Considering the working capacities of the triple beam irradiation facility, the best possible combination turned out to be 8 MeV Si, 2 MeV He, and 0.333 MeV H ions, at fluences corresponding to 0.75 year-long working period in the first wall location. In addition, we took advantage of the opportunity of using Al energy degraders along the path of the He beam to obtain a more homogeneous implantation profile of these ions, which are expected to be the most abundant species produced by transmutation (all the experimental details are given in the next section). The above-mentioned permanence at the first wall location induces 4.4 dpa, 76 appm He/dpa and 4.5 appm H/dpa, as predicted by PHITS. The computation was carried out by the SRIM-2013 code [21] using the Kinchin-Pease approach [22].

Si and H ions were assumed to directly impact on the glass ceramic materials under the angle of 15°, as from the JANNuS-Saclay facility design. On the contrary, the profile of the implanted He ions was evaluated in two steps. First, for each Al

foil thickness we evaluated the He scattering on Al degraders and information of the consequent divergence of the emerging beam were computed. Then, these results were used as input to simulate the impact of the He scattered beam on the glass-ceramic target (with 15° angle) and calculate the implantation profile. We estimated the effective fraction of He ions that reaches the target considering the target diameter and its position with respect to the degraders. The percentage of He-ion implanting in the rotating wheel on which the degraders are mounted were taken into account as well.

Figure 1 shows the depth profile of the displacement damage and of the He and H concentration obtained for a Si, He and H fluence of 2.6×10^{16} cm^{-2}, 9.8×10^{15} cm^{-2} and 9.0×10^{13} cm^{-2} respectively. The dpa contribution from He and H beams were found to be negligible, therefore the dpa values are given from Si ion irradiation only.

The displacement damage is not homogeneous and reaches the wanted value of 4.4 dpa in correspondence of the H implantation peak. Five different peaks are visible in the He implantation profile corresponding to the five energy degradation levels used in the experiment. Since a position on the degrader wheel is empty there is a sixth peak due to He ions not slowed down, but it is located at a depth greater than 5 μm, namely outside the frame of the figure. The simulated irradiation configuration provides a appm He/dpa and appm H/dpa ratios of $\sim$ 72 and $\sim$ 10, respectively, in correspondence to the H implantation peak. If the He concentration corresponds to that predicted by the PHITS simulation, the H concentration is about double. However, account should be taken of the possible migration of the gas in high temperature irradiation experiment with the consequent homogeneization and reduction of the H abundance.

3. Experiments

3.1. CA glass-ceramic preparation

The CA glass was synthesised by melting/quenching: the powdered raw products ($CaCO_3$ and Al_2O_3) were melted in a platinum-rhodium crucible in air at 1650°C for 1h (in batches of 50 g), then the glass was poured on a brass plate and subsequently powdered and sieved as explained in details elsewhere [23, 24, 12, 25]. Three pellets with an average diameter of 8.10 mm and a thickness of 2.90 mm were then prepared by a devitrification process; more in details, the pellets were prepared by uniaxially pressing a mixture of glass powders (grain size 38-75 μm) and isopropyl alcohol; the obtained pellet was subsequently sintered at 1480°C for 10 min in an oven in Ar atmosphere. As a final process, the parallel surfaces of the pellet were polished using SiC papers (grits 600/800/1000/1200/2500/4000). The density of the glass-ceramic was calculated using Archimede's method.

3.2. Irradiation

Irradiation experiments were performed at the JANNuS-Saclay facility, making simultaneously use of the three electrostatic accelerators available, respectively named Épiméthée, Japet and Pandore, connected to a triple beam chamber [26, 27]. Épiméthée is a 3 MV, single-ended Pelletron equipped with an electron cyclotron resonance source that, for the present experiment, delivered 2 MeV He^+ ions. The He^+ particles were partially slowed by means of energy-degraders (Al foils) of different thicknesses (3, 3.4, 3.8, 4.4 and 5 μm) mounted on a rotating stage, in order to achieve a homogeneous distribution over a quite large depth. Japet is a 2 MV Tandem equipped with an external Cs sputtering source, which provided 8 MeV Si^{3+} ions. Pandore is a 2.5 MV, single-ended equipped with a RF source which delivered 0.333 MeV protons. The triple beam chamber receives one beamline coming from each accelerator with an incidence angle of 15°, allowing triple beam irradiations. During irradiation experiment, current intensity was monitored using a mobile multi-pin Faraday cups device, yielding an accurate quantification of implanted species. Pumping groups and cold traps allowed reaching a vacuum better than 10^{-7} Torr, while a heating stage provided precise temperature control at 400°C, 615°C and 710°C, respectively. The temperature was measured by thermocouples positioned in contact with the sample, while its uniformity was continuously checked by a 2D infrared thermal imaging camera. The temperatures chosen were the closest, experimentally accessible, to the expected operation conditions [2]. During irradiation experiments, the three ion beams were continuously synchronized to maintain the fluence ratios. Experiments were performed for about 6 hours.
The irradiation conditions for the three CA samples are summarized in Table 2. A circular area with a diameter of 7.0 mm was homogeneously irradiated on each sample.

Irradiation T (°C)	Si fluence (cm^{-2})	He fluence (cm^{-2})	H fluence (cm^{-2})
400	$(2.6\pm0.3)\times10^{16}$	$(9.9\pm1.5)\times10^{15}$	$(8.8\pm0.9)\times10^{13}$
615	$(2.6\pm0.3)\times10^{16}$	$(9.9\pm1.5)\times10^{15}$	$(10.0\pm1.0)\times10^{13}$
710	$(2.6\pm0.3)\times10^{16}$	$(9.9\pm1.5)\times10^{15}$	$(7.3\pm0.7)\times10^{13}$

Table 2: Summary of the irradiation conditions for the three CA samples.

3.3. TEM analysis

Cross-sectional specimens were extracted as lamellae (perpendicular to the sample surface, including both irradiated and pristine regions) for TEM analysis using focused ion beam (FIB) milling in a FEI HeliosNanolab FIB/SEM. Prior to milling a protective layer of platinum was deposited on the top surface, over the irradiated region. STEM-EDX was carried out in a FEI Osiris (200 kV acceleration voltage) equipped with a high-brightness X-FEG gun and a Bruker Super-X EDX detector. EDX maps were acquired with sampling every 50 nm and a dwell time of 50 ms per pixel, using a beam current of 600 pA. Resistance to beam damage was verified by repeated scanning over the same areas, which did not show differences in elemental distribution. EDX spectrum images were denoised using the PCA routines implemented in Hyperspy, and the elemental maps were extracted using the same software suite.

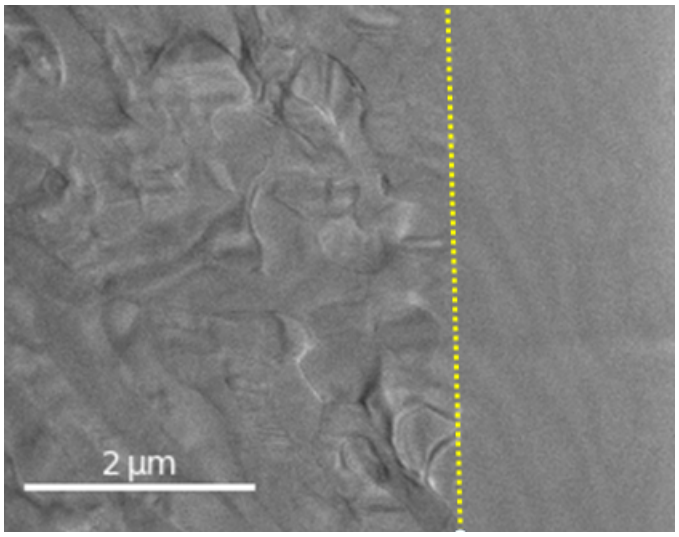

Figure 2: TEM image of the interface between pristine (left side, deeper in the pellet) and irradiated (right side, closer to the surface) portions of the CA sample irradiated at 400°C.

4. Results and discussion

The TEM analysis allows us to discuss the radiation damage and the nature of induced defects. In particular, we focus on the amorphization and phase mixing of the glass-ceramic due to dpa and heating, and on the formation of bubbles/cavities due to the presence of He and H. Moreover, their trends as a function of irradiation temperature are discussed. For clarity and brevity, the shown images refer to the two extremal temperatures, the analysis of the intermediate temperature case confirms the displayed trends.

4.1. Amorphization

The high dpa level introduced in the pellets results in an amorphization of the glass-ceramic material. The effect is clearly visible in the cross-sectional lamellae (as shown in fig. 2). Due to the fact that deep in the pellets (after the implantation depth of the ions) the material is still in the pristine state, it is possible to compare the same sample in the two conditions. The interface between the amorphized and the pristine areas appears well defined and sharp (less than a few tens of nm) in all samples. While in most cases this interface is parallel to the surface of the sample (i.e. at a fixed depth), in the sample irradiated at the highest temperature the amorphous front follows the profile of underlying grains. This could possibly be determined by a partial re-crystallization of some grains resulting from the enhanced mobility of displaced atoms at high temperature and during irradiation. In fact it was reported that the diffusion coefficient is enhanced during beam exposure [28, 29]. To locally assess the crystallinity, electron diffraction patterns were taken at increasing depth in STEM microprobe configuration. This setup results in an electron probe a few nm in size, allowing the acquisition of diffraction patterns from a small region. The results (see Fig. 3) clearly show a sharp loss of crystallinity:

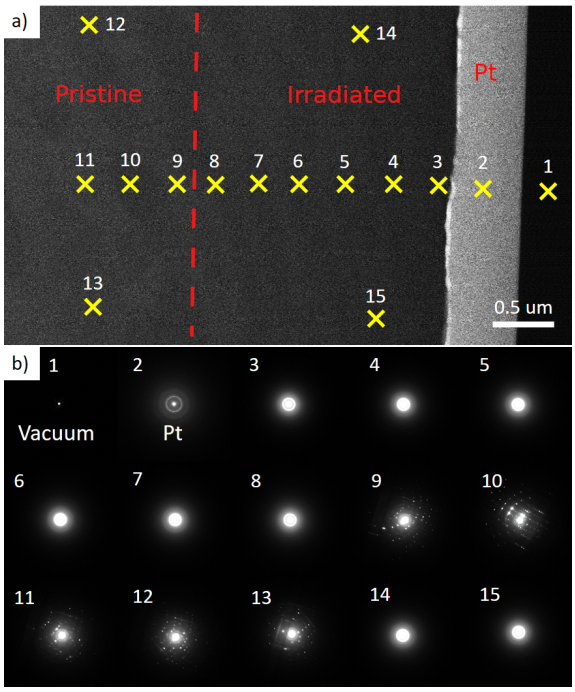

Figure 3: a) STEM image of the CA sample irradiated at 400°C with numbered positions where the diffraction patterns were taken. b) Diffraction patterns showing the amorphization of the glass-ceramic in the irradiated area. Note the abrupt transition between positions 8 and 9.

Sample and phase	Al at%	Ca at%	O at%
Pristine - phase 1	24.5	11.1	64.3
400°C - phase 1	27.0	13.1	59.9
710°C - phase 1	25.0	13.9	61.1
Theoretical $CaAl_2O_4$	28.6	14.3	57.1
Pristine - phase 2	19.6	23.7	56.7
400°C - phase 2	19.1	24.6	56.3
710°C - phase 2	19.0	23.4	57.6
Theoretical $Ca_3Al_2O_6$	18.2	27.3	54.5

Table 3: Elemental composition from STEM-EDX for both phases in all samples, including reference values for expected phases.

specifically, the patterns are predominantly amorphous until the pristine area is reached, where clear single-crystal spot patterns can be seen.
Noticeably, the same effect was observed in CA irradiated with Si alone (without He and H implantation) and does not alter the jointing properties of the material [16].

4.2. Phase mapping via STEM-EDX and identification using diffraction

Compositional analysis using STEM-EDX revealed the presence of two distinct phases in the pristine material, with differences in the Al and Ca contents. The two phases correspond to the Al-rich and Ca-rich areas shown in STEM-HAADF image (Fig. 4) ; the composition of the two phases, shown in table 3, are compatible with $Ca_3Al_2O_6$ and $CaAl_2O_4$ within the expected accuracy of a few percent for EDX quantification.

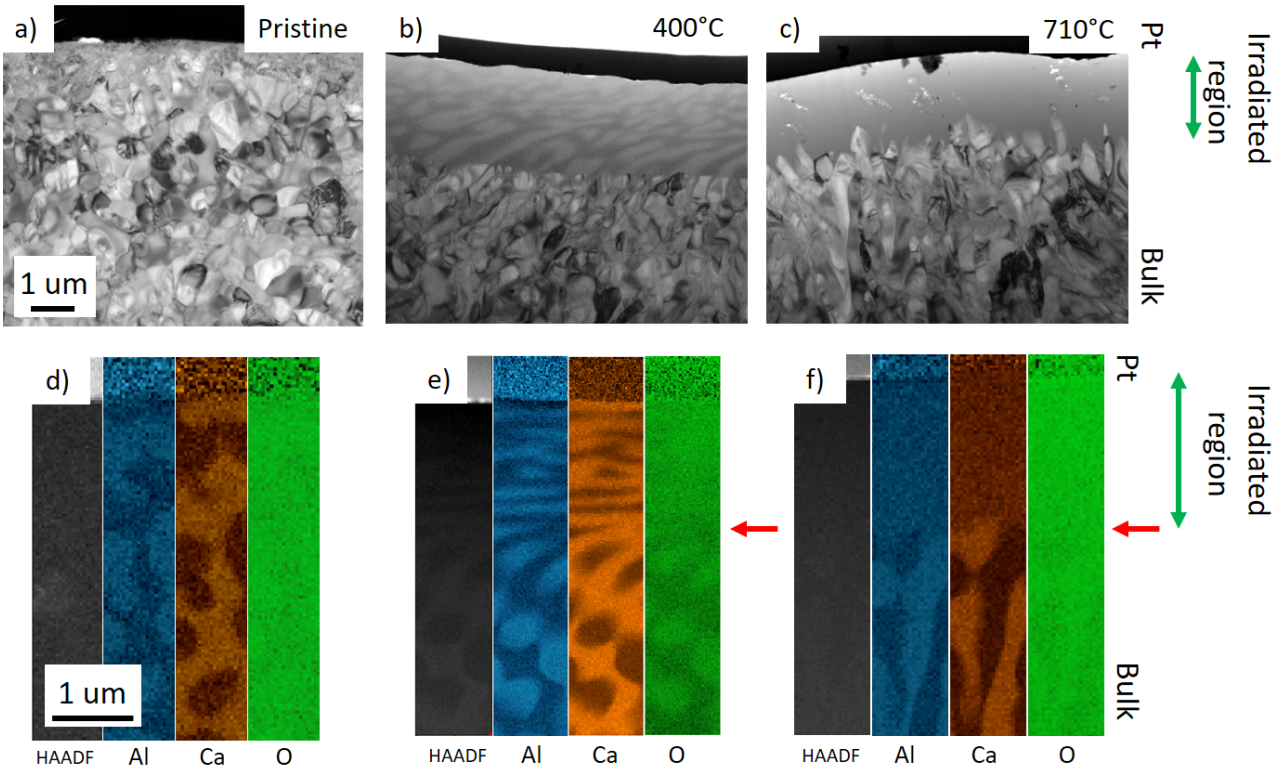

Figure 4: Comparison of TEM cross-sectional views of samples: a) pristine, b) 400°C, c) 710°C. The amorphized area is visible as a homogeneous layer under the surface. The original top surface of the sample is the interface with the Pt layer at the top of each image. Panels d-e-f report STEM-HAADF images and elemental maps for Al, Ca and O; the interface between the amorphous and crystalline areas is highlighted by red arrows. The scale bars apply to all panels on each row.

As visible in Fig. 4, the irradiated area in the sample treated at 400°C appears as a not homogeneous (a preservation of two chemical phases is clearly visible) amorphous phase, indicating the persistence of phase separation, despite the amorphization. However, a clear distortion occurs. The preferential direction of smearing in the horizontal plane might be due to the slab-like geometry of the irradiated portion of the sample, where mobility is enhanced (as discussed above). It can be suggested that the rate of dissolution and the precipitation reaction at the irradiated-pristine interface (determined by the irradiation) produces a change in the shape of the grains, which are elongated in the direction along the interface [30]. In the case of irradiation at higher temperature the two phases are no longer distinct; this could be once again determined by the increased mobility of species at higher temperature; it can be speculated that the not homogeneous amorphous phase observed at lower temperature evolves to a homogeneous glassy phase at higher T because an irradiation promoted solubility process of the two amorphous phase begins to occur.

Moreover, at high temperature (Fig. 4 c) the interface between the irradiated area and pristine area is not sharp, contrasting to what observed in CA sample irradiated at lower temperature (Fig. 4 b). This supports the speculation that mobility is increased by both irradiation and high temperature, leading to a recrystallization phenomenon (in Figure 4 c, crystals are formed in the glassy matrix, across the separation line between the irradiated and not-irradiated area). The fact that the pristine regions of the irradiated samples do not show any of these phenomena clearly indicates that they are necessarily due to the irradiation rather than to the thermal history of the glass-ceramic. Using selected area electron diffraction the phases were confirmed to be $Ca_3Al_2O_6$ and $CaAl_2O_4$ (Fig. 5). No other phases were observed among the crystalline areas.

4.3. Bubbles

Transmutation induced presence of He and H was emulated by controlled gas implantation. The presence of these elements can result in the formation of bubbles and cavities in the target material that in principle might be detrimental for the mechanical properties. Indeed, as shown in Fig. 6, we find that irradiation induced the formation of structures appearing lighter than the surrounding region in TEM images, which might be either cavities or gas-filled bubbles. Their presence is more marked in the areas irradiated at the higher temperatures, where these features are about 10 nm in size and aggregate in clusters. These structures are absent in the pristine portions of the material and were not observed in CA irradiated with Si alone [16], indicating the importance of multibeam experiments.

4.4. Trends in T

The irradiation temperature is found to play an important role in the determination of the structural effects on glass-ceramic samples, possibly due to the higher mobility of both

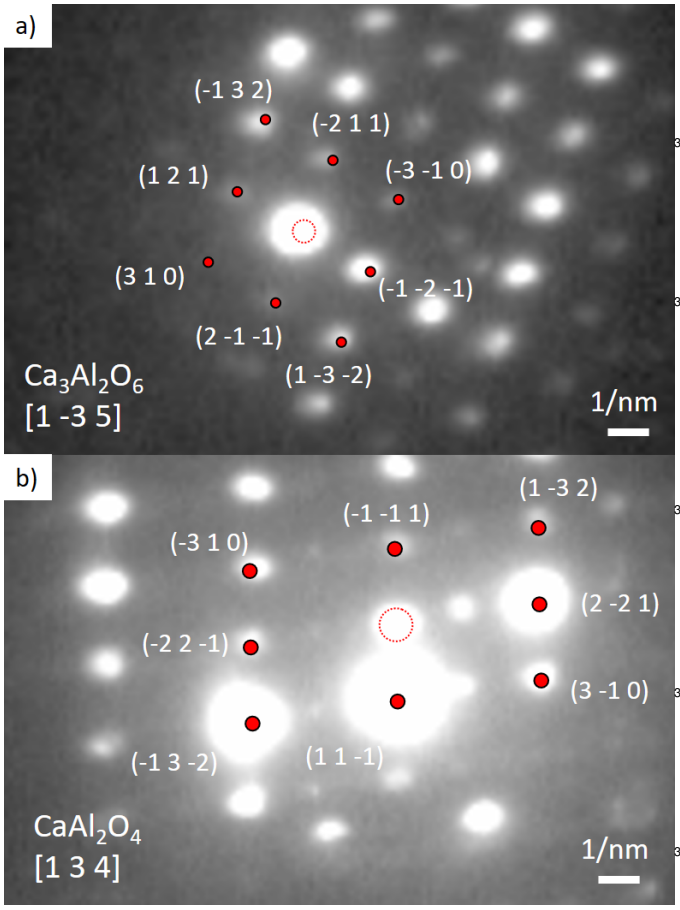

Figure 5: Selected area diffraction patterns acquired from single crystals of the two phases on the CA sample irradiated at 400°C: a) $Ca_3Al_2O_6$, b) $CaAl_2O_4$. The zone axis pattern of the crystal is superimposed on the image.

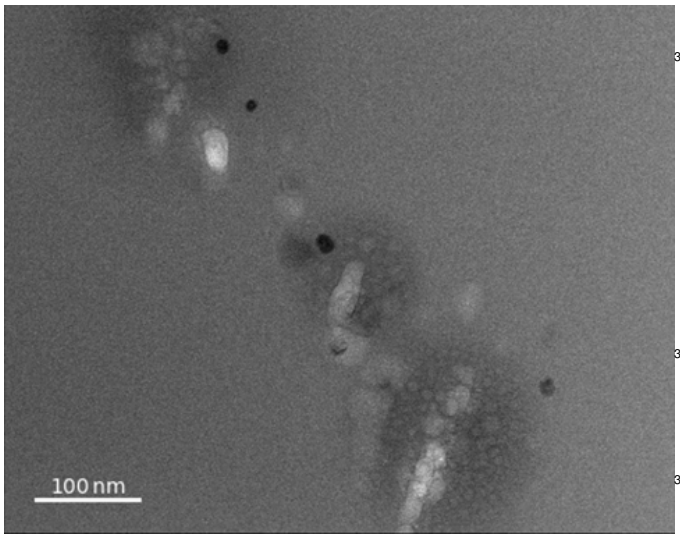

Figure 6: TEM image of bubbles/cavities in the irradiated portion of the CA sample irradiated at 710°C.

ions and aggregates. We observed that, while some amorphization is always present in the irradiated area, at 710° C partial recrystallization of some grains seems to take place at the interface with the pristine region. In addition, the phase mixing increases with the irradiation temperature, up to the point that in the sample irradiated at 710° C no separate phases are visible in the irradiated area. Finally, the number of bubbles/cavities increases with the irradiation temperature, and for the highest temperature results even in micrometer-scale clusters. This result agrees with the output of atomistic simulations investigating the formation and aggregation of He bubbles in materials for fusion technology. Indeed, such calculations have shown that these processes are temperature dependent: the higher the temperature, the faster He atoms and clusters diffuse, promoting coalescence [31].

5. Conclusions

In summary, we investigated the effects of high flux and high energy neutron irradiations (conditions relevant for future nuclear fusion reactors) on a glass-ceramic material through the introduction of the expected defects distribution via triple ion irradiation. The calcia-alumina samples were irradiated at temperatures ranging from 400° C to 710° C, with 8 MeV Si, 2 MeV He, and 0.333 MeV H ions, at fluences corresponding to 0.75 year-long working period in the DEMO first wall location. This combination of ions and energies was chosen to reproduce as closely as possible the damage expected by 14 MeV neutrons in terms of dpa and transmutation products (He and H) as evaluated by Monte Carlo simulations. The TEM analysis, imaging accompanied by EDX and diffraction, highlighted that the irradiation temperature plays a prominent role in determining the induced damage in terms of recrystallization, phase mixing and bubble formation. This study identified the type of defects to be expected in glass-ceramic materials at the working conditions for fusion technology. Each of these defects should be investigated in terms of their impact on mechanical properties on large samples of joined SiC pieces.

Acknowledgements

This research did not receive any specific grant from funding agencies in the public, commercial, or not-for-profit sectors.

References

[1] D. Guo, H. Zang, C. He, P. Zhang, T. Li, X. Cao, L. Ma, Preliminary studies on the emulation of 14 MeV neutron irradiation in SiC with heavy ions, Fusion Engineering and Design 100 (2015) 274–279. doi:https://doi.org/10.1016/j.fusengdes.2015.06.085. URL https://www.sciencedirect.com/science/article/pii/S0920379615301149

[2] A. Rowcliffe, L. Garrison, Y. Yamamoto, L. Tan, Y. Katoh, Materials challenges for the fusion nuclear science facility, Fusion Engineering and Design 135 (2018) 290–301, special Issue: FESS-FNSF Study. doi:https://doi.org/10.1016/j.fusengdes.2017.07.012. URL https://www.sciencedirect.com/science/article/pii/S0920379617307524

[3] S. Zinkle, G. Was, Materials challenges in nuclear energy, Acta Materialia 61 (3) (2013) 735–758, the Diamond Jubilee Issue. doi:https://doi.org/10.1016/j.actamat.2012.11.004.
URL https://www.sciencedirect.com/science/article/pii/S1359645412007987

[4] Y. Katoh, L. L. Snead, Silicon carbide and its composites for nuclear applications – historical overview, Journal of Nuclear Materials 526 (2019) 151849. doi:https://doi.org/10.1016/j.jnucmat.2019.151849.

[5] Y. Katoh, L. Snead, C. Henager, T. Nozawa, T. Hinoki, A. Iveković, S. Novak, S. Gonzalez de Vicente, Current status and recent research achievements in SiC/SiC composites, Journal of Nuclear Materials 455 (1) (2014) 387–397, proceedings of the 16th International Conference on Fusion Reactor Materials (ICFRM-16). doi:https://doi.org/10.1016/j.jnucmat.2014.06.003.
URL https://www.sciencedirect.com/science/article/pii/S0022311514003602

[6] L. Nuckols, M. L. Crespillo, C. Xu, E. Zarkadoula, Y. Zhang, W. J. Weber, Coupled effects of electronic and nuclear energy deposition on damage accumulation in ion-irradiated sic, Acta Materialia 199 (2020) 96–106. doi:https://doi.org/10.1016/j.actamat.2020.08.014.
URL https://www.sciencedirect.com/science/article/pii/S135964542030611X

[7] T. Koyanagi, Y. Katoh, T. Nozawa, Design and strategy for next-generation silicon carbide composites for nuclear energy, Journal of Nuclear Materials 540 (2020) 152375. doi:https://doi.org/10.1016/j.jnucmat.2020.152375.

[8] T. Koyanagi, Y. Katoh, T. Nozawa, L. Snead, S. Kondo, C. Henager, M. Ferraris, T. Hinoki, Q. Huang, Recent progress in the development of SiC composites for nuclear fusion applications, Journal of Nuclear Materials 511 (2018) 544–555, special Section on "18th International Conference on Fusion Reactor Materials". doi:https://doi.org/10.1016/j.jnucmat.2018.06.017.
URL https://www.sciencedirect.com/science/article/pii/S0022311518301995

[9] L. Snead, T. Nozawa, M. Ferraris, Y. Katoh, R. Shinavski, M. Sawan, Silicon carbide composites as fusion power reactor structural materials, Journal of Nuclear Materials 417 (1) (2011) 330–339, proceedings of ICFRM-14. doi:https://doi.org/10.1016/j.jnucmat.2011.03.005.

[10] M. Salvo, V. Casalegno, S. Rizzo, F. Smeacetto, A. Ventrella, M. Ferraris, 17 - glasses and glass-ceramics as brazing materials for high-temperature applications, in: D. P. Sekulić (Ed.), Advances in Brazing, Woodhead Publishing Series in Welding and Other Joining Technologies, Woodhead Publishing, 2013, pp. 525–544. doi:https://doi.org/10.1533/9780857096500.3.525.
URL https://www.sciencedirect.com/science/article/pii/B9780857094230500171

[11] M. Ferraris, M. Salvo, V. Casalegno, A. Ciampichetti, F. Smeacetto, M. Zucchetti, Joining of machined SiC/SiC composites for thermonuclear fusion reactors, Journal of Nuclear Materials 375 (3) (2008) 410–415. doi:https://doi.org/10.1016/j.jnucmat.2008.02.020.
URL https://www.sciencedirect.com/science/article/pii/S0022311508001062

[12] M. Ferraris, M. Salvo, V. Casalegno, S. Han, Y. Katoh, H. Jung, T. Hinoki, A. Kohyama, Joining of SiC-based materials for nuclear energy applications, Journal of Nuclear Materials 417 (1) (2011) 379–382, proceedings of ICFRM-14. doi:https://doi.org/10.1016/j.jnucmat.2010.12.160.
URL https://www.sciencedirect.com/science/article/pii/S0022311510009827

[13] H. Kishimoto, K. Ozawa, O. Hashitomi, A. Kohyama, Microstructural evolution analysis of nite SiC/SiC composite using tem examination and dual-ion irradiation, Journal of Nuclear Materials 367-370 (2007) 748–752, proceedings of the Twelfth International Conference on Fusion Reactor Materials (ICFRM-12). doi:https://doi.org/10.1016/j.jnucmat.2007.03.043.

[14] M. Ferraris, V. Casalegno, S. Rizzo, M. Salvo, T. Van Staveren, J. Matejicek, Effects of neutron irradiation on glass ceramics as pressure-less joining materials for SiC based components for nuclear applications, Journal of Nuclear Materials 429 (1) (2012) 166–172. doi:https://doi.org/10.1016/j.jnucmat.2012.05.035.

[15] L. Gozzelino, V. Casalegno, G. Ghigo, T. Moskalewicz, A. Czyrska-Filemonowicz, M. Ferraris, He-irradiation effects on glass-ceramics for joining of SiC-based materials, Journal of Nuclear Materials 472 (2016) 28–34. doi:https://doi.org/10.1016/j.jnucmat.2016.01.024.
URL https://www.sciencedirect.com/science/article/pii/S0022311516300228

[16] V. Casalegno, S. Kondo, T. Hinoki, M. Salvo, A. Czyrska-Filemonowicz, T. Moskalewicz, Y. Katoh, M. Ferraris, CaO-Al2O3 glass-ceramic as a joining material for SiC based components: A microstructural study of the effect of Si-ion irradiation, Journal of Nuclear Materials 501 (2018) 172–180. doi:https://doi.org/10.1016/j.jnucmat.2018.01.033.
URL https://www.sciencedirect.com/science/article/pii/S0022311517312928

[17] S. Yang, Y. Nakagawa, M. Kondo, T. Shibayama, Anisotropic defect distribution in he+-irradiated 4h-sic: Effect of stress on defect distribution, Acta Materialia 211 (2021) 116845. doi:https://doi.org/10.1016/j.actamat.2021.116845.
URL https://www.sciencedirect.com/science/article/pii/S1359645421002251

[18] E. Aradi, J. Lewis-Fell, G. Greaves, S. Donnelly, J. Hinks, In situ tem investigations of the microstructural changes and radiation tolerance in sic nanowhiskers irradiated with he ions at high temperatures, Acta Materialia 210 (2021) 116820. doi:https://doi.org/10.1016/j.actamat.2021.116820.
URL https://www.sciencedirect.com/science/article/pii/S1359645421002007

[19] S. G. de Vicente, J.-L. Boutard, S. Zinkle, H. Tanigawa, Materials testing facilities and programmes for fission and ion implantation damage, Nuclear Fusion 57 (9) (2017) 092011. doi:10.1088/1741-4326/aa6a67.
URL https://doi.org/10.1088/1741-4326/aa6a67

[20] T. Sato, K. Niita, N. Matsuda, S. Hashimoto, Y. Iwamoto, S. Noda, T. Ogawa, H. Iwase, H. Nakashima, T. Fukahori, K. Okumura, T. Kai, S. Chiba, T. Furuta, L. Sihver, Particle and heavy ion transport code system, phits, version 2.52, Journal of Nuclear Science and Technology 50 (9) (2013) 913–923. doi:10.1080/00223131.2013.814553.

[21] J. F. Ziegler, M. Ziegler, J. Biersack, Srim – the stopping and range of ions in matter (2010), Nuclear Instruments and Methods in Physics Research Section B: Beam Interactions with Materials and Atoms 268 (11) (2010) 1818–1823, 19th International Conference on Ion Beam Analysis. doi:https://doi.org/10.1016/j.nimb.2010.02.091.
URL https://www.sciencedirect.com/science/article/pii/S0168583X10001862

[22] R. Stoller, M. Toloczko, G. Was, A. Certain, S. Dwaraknath, F. Garner, On the use of srim for computing radiation damage exposure, Nuclear Instruments and Methods in Physics Research Section B: Beam Interactions with Materials and Atoms 310 (2013) 75–80. doi:https://doi.org/10.1016/j.nimb.2013.05.008.
URL https://www.sciencedirect.com/science/article/pii/S0168583X13005053

[23] M. Ferraris, M. Salvo, C. Isola, M. Appendino Montorsi, A. Kohyama, Glass-ceramic joining and coating of SiC/SiC for fusion applications, Journal of Nuclear Materials 258-263 (1998) 1546–1550. doi:https://doi.org/10.1016/S0022-3115(98)00176-7.
URL https://www.sciencedirect.com/science/article/pii/S0022311598001767

[24] Y. Katoh, M. Kotani, A. Kohyama, M. Montorsi, M. Salvo, M. Ferraris, Microstructure and mechanical properties of low-activation glass-ceramic joining and coating for SiC/SiC composites, Journal of Nuclear Materials 283-287 (2000) 1262–1266, 9th Int. Conf. on Fusion Reactor Materials. doi:https://doi.org/10.1016/S0022-3115(00)00096-9.
URL https://www.sciencedirect.com/science/article/pii/S0022311500000969

[25] M. Ferraris, M. Salvo, S. Rizzo, V. Casalegno, S. Han, A. Ventrella, T. Hinoki, Y. Katoh, Torsional shear strength of silicon carbide components pressurelessly joined by a glass-ceramic, International Journal of Applied Ceramic Technology 9 (4) (2012) 786–794. arXiv:https://ceramics.onlinelibrary.wiley.com/doi/pdf/10.1111/j.1744-7402.2012.02775.x, doi:https://doi.org/10.1111/j.1744-7402.2012.02775.x.

URL https://ceramics.onlinelibrary.wiley.com/doi/abs/10.1111/j.1744-7402.2012.02775.x

[26] L. Beck, Y. Serruys, S. Miro, P. Trocellier, E. Bordas, F. Leprêtre, D. Brimbal, T. Loussouarn, H. Martin, S. Vaubaillon, et al., Ion irradiation and radiation effect characterization at the JANNUS-Saclay triple beam facility, Journal of Materials Research 30 (9) (2015) 1183–1194. doi:https://doi.org/10.1557/jmr.2014.414.

[27] A. Gentils, C. Cabet, Investigating radiation damage in nuclear energy materials using JANNuS multiple ion beams, Nuclear Instruments and Methods in Physics Research Section B: Beam Interactions with Materials and Atoms 447 (2019) 107–112. doi:https://doi.org/10.1016/j.nimb.2019.03.039.
URL https://www.sciencedirect.com/science/article/pii/S0168583X19301697

[28] A. Martinavičius, G. Abrasonis, W. Möller, C. Templier, J. P. Rivière, A. Declémy, Y. Chumlyakov, Anisotropic ion-enhanced diffusion during ion nitriding of single crystalline austenitic stainless steel, Journal of Applied Physics 105 (9) (2009) 093502. doi:10.1063/1.3120912.
URL https://doi.org/10.1063/1.3120912

[29] T. Chen, Y. Yang, L. He, B. Tyburska-Püschel, K. Sridharan, H. Xu, L. Tan, Enhanced diffusion of Cr in 20Cr-25Ni type alloys under proton irradiation at 670°C, Nuclear Materials and Energy 17 (2018) 142–146. doi:https://doi.org/10.1016/j.nme.2018.10.001.
URL https://www.sciencedirect.com/science/article/pii/S2352179118301029

[30] R. Raj, C. Chyung, Solution-precipitation creep in glass ceramics, Acta Metallurgica 29 (1) (1981) 159–166. doi:https://doi.org/10.1016/0001-6160(81)90096-1.
URL https://www.sciencedirect.com/science/article/pii/0001616081900961

[31] D. Stewart, Y. Osetskiy, R. Stoller, Atomistic studies of formation and diffusion of helium clusters and bubbles in bcc iron, Journal of Nuclear Materials 417 (1) (2011) 1110–1114, proceedings of ICFRM-14. doi:https://doi.org/10.1016/j.jnucmat.2010.12.217.
URL https://www.sciencedirect.com/science/article/pii/S0022311510010391